Assessment of the infection risk distribution of COVID-19 and ventilation energy consumptions in indoor environments

Marco Marigo [a], *Giacomo* Tognon [a], *Michele* De Carli [a], *Angelo* Zarrella [a]

[a] Department of Industrial Engineering, University of Padova, Italy. E-mail: marco.marigo.3@studenti.unipd.it

Abstract. The energy use for ventilating buildings involves high economic and primary energy consumption costs. Nevertheless, ventilation is essential, especially in public places, to ensure acceptable Indoor Air Quality (IAQ) levels and reduce the risk of airborne virus infection. The latter aspect has recently increased because of the ongoing COVID-19 pandemic. In this paper, a model that couples a zonal ventilation model with infection risk calculation is integrated with an energy consumption model to analyse the energy consumption and infection risk from COVID-19 at different ventilation flow rates for three case studies: an office room, a high school and a university classroom. The main results show that the increase in ventilation flow rate involves reducing risk, but it increases energy consumption. Moreover, the mask-wearing resulted in having a relevant effect, whereas the effect of the relative position difference inside the room was not detected with the proposed discretisation.

Keywords. HVAC, risk assessment, COVID-19, ventilation, indoor air quality, energy consumption, building energy model.
DOI: https://doi.org/10.34641/clima.2022.80

1. Introduction

Buildings are one of the leading energy consumption sectors in Europe. In 2018, they were responsible for 40% of final energy use and the consequent greenhouse gas emissions into the atmosphere, leading to a significant environmental impact [1].

People spend most of their time in indoor spaces, so fulfilling a good indoor environmental quality (IEQ) is primarily important to guarantee their wellness. Thermal comfort and indoor air quality (IAQ) are provided by the HVAC system of the building. In particular, the supply of outdoor air by ventilation is fundamental to replace stale indoor air, thus removing pollutants. In the case of mechanically ventilated buildings (full-air or primary air systems), the consumptions are those related to air handling unit operation, namely thermal energy required at the heating and cooling coils and fan electrical absorption to supply it to the indoor environment.

The salubrity of indoor environments has become the main topic with the beginning of the COVID-19 pandemic, caused by the spread of SARS-CoV-2, whose existence was first reported to the WHO Country Office in China on 31st December 2019 [2]. According to the current knowledge, the disease transmission mainly occurs by contact with infected subjects or contaminated surfaces (fomites) and large exhaled droplets [3]. The airborne transmission caused by suspended virus-laden microdroplets is a third possibility. Its relevance in indoor environments is increasingly recognised after the documentation of COVID-19 outbreaks [4,5].

The airborne infection route is the result of subsequent phases: infectious aerosol generation, transport and inhalation [6]. Droplet nuclei are generated by the infected subject through common respiratory activity, such as breathing, talking, coughing, sneezing. Ventilation and air distribution systems play a key role in transporting pathogens, determining their spread across the available space, dilution and removal. Therefore, ventilation has been immediately recommended as a suitable mitigation strategy against the airborne transmission of the disease, along with personal protection devices and social distancing [3].

Different approaches have been proposed to model the airborne transmission of respiratory diseases in indoor spaces. All methods aim at determining the concentration of infectious material that a susceptible individual could inhale. The most accurate analyses are provided by CFD simulations, as they can define precisely the airflow patterns, but they require high computational resources [7]. On the other hand, simple mathematical models have been developed to calculate the airborne infection risk and investigate the effectiveness of the countermeasures. Among these, the Wells-Riley

Copyright ©2022 by the authors. This conference paper is published under a CC-BY-4.0 license.

equation and its modifications are widely used for the current pandemic. It is based on the concept of infectious quantum, a hypothetical dose unit that makes 63.2% of an exposed population sick. The indoor space is considered as perfectly mixed and an exponential probability equation is used to calculate risk [8]. Despite their simplicity, they can be used to quickly estimate suitable ventilation rates for risk mitigation in a given situation.

Nevertheless, risk models do not consider the energy needs for air handling associated with an increase in the air change rates. Recently, several researchers have focused on the double effect of ventilation rate on infection and energy consumptions trends. Schibuola and Tambani estimated the reproduction number (number of secondary infections per infected person) in two naturally ventilated Italian schools, by monitoring the CO_2 concentration. They proposed an high efficiency air handling unit to achieve both risk mitigation and contained energy needs [9]. Wang et al. analysed the effectiveness of a smart ventilation control based on occupant density in mitigating the airborne transmission of SARS-CoV-2 and saving ventilation energy. Compared to a traditional system with fixed outdoor air ratio, the infection probabilty was lowered up to 2 %, and 11.7 % of consumptions saving was obtained [10].

This paper evaluates the effect of outdoor air supply on infection risk and energy consumption. For the first aspect, a risk zonal model for assessing the infection probability from COVID-19 in indoor environments is presented. It originates from the need to abandon the usual assumption of a well-mixed space since it involves a macro-discretisation of the interested domain into different cells, as proposed in [11]. The main purposes are analysing the effect of increasing the ventilation flow rate on airborne transmission and observing the spatial variation of risk. Successively, the rise in the energy needs for air handling is determined to investigate the drawbacks of this mitigation strategy. The model has also been applied to verify the benefits of wearing masks in lowering infection risk. In Section 2, the model and calculation method are illustrated. The procedure is applied to three different single rooms; the case studies are presented in Section 3. Finally, the obtained results and considerations are summarised in Section 4.

2. Method

In this section, the development of a risk zonal model is presented. It couples a zonal ventilation model to the infection risk calculation. The former applies a macro-discretisation of the indoor space into multiple cells in order to define the interzonal airflows transporting the infectious aerosols. The second step assesses the airborne infection probability within each cell through a risk equation.

2.1 Zonal ventilation model

The application of the zonal model is aimed at the definition of the air movements within the environment concerned. It provides an intermediate approach between nodal modelling and CFD analyses [12]. The POMA model (Pressurized ZOnal Model with Air Diffuser) was applied in this work (Haghighat et al., 2001), whose principle is to subdivide the geometrical domain into well-mixed cells or zones.

The model is founded on some basic assumptions. The discretisation grid comprises parallelepiped-shaped cells, so there are only vertical and horizontal interfaces. Each zone is well-mixed in temperature and density, whereas the pressure is hydrostatically distributed, starting from a reference value at the bottom level. The thermodynamic properties are correlated by the ideal gas law.

Regions affected by thermal plumes and wall boundary layers are not modelled. Jets model does not consider the spatial effect, but supply and return airflows are assumed as input parameters in the mass balances of the zones where diffusers and grilles are placed. Therefore, each cell is surrounded by two types of boundary surfaces: normal interfaces of separation with adjacent zones, and, for the outer zones, wall boundaries interested only by heat exchanges. Mass and heat flows are modelled for each boundary.

As regards the interzonal mass flows, they are calculated as a function of the static pressure difference across the normal boundary, through the well-known Power Law (Eq. (1)):

$$\dot{m} = \rho\, k\, A\, \Delta P^n \qquad (1)$$

Parameters k and n are the flow coefficient (i.e., permeability of the boundary) and the flow exponent, respectively. For k, a value of 0.83 m s^{-1} Pa^{-n} is taken from previous studies [13], while for n a value of 0.5 is assigned considering turbulent airflow.

The horizontal boundaries present a constant pressure difference along the interface, between the reference pressure of the upper zone and the pressure at the summit of the lower one. Conversely, vertical boundaries are characterised by a variable pressure difference along the surface due to the linear pressure distributions at both sides (Fig.1).

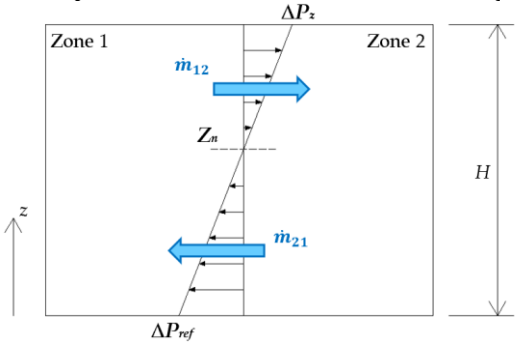

Fig. 1 – Vertical pressure distribution and neutral plane between adjacent cells.

In this case, a neutral plane Z_n is defined as the height at which opposite pressures equalise, leading to a null horizontal airflow across that point. The neutral plane position is determined through Eq. (2), and the mass flowrates, above and below it, are calculated integrating the Power Law along the vertical coordinate (Eqs. (3)-(4)):

$$Z_n = \frac{\Delta P_{ref}}{g\,\Delta\rho} \tag{2}$$

$$\dot{m}_{0-Z_n} = \rho_{0-Z_n}\, k\, L\, |g\,\Delta\rho|^n\, \frac{|Z_n|^{n+1}}{n+1} \tag{3}$$

$$\dot{m}_{Z_n-H} = \rho_{Z_n-H}\, k\, L\, |g\,\Delta\rho|^n\, \frac{|Z_n-H|^{n+1}}{n+1} \tag{4}$$

where L is the depth of the vertical interface, $m_{0\text{-}Zn}$ is the mass flowrate crossing the interface portion from 0 to Z_n, whereas $m_{Zn\text{-}H}$ is that crossing the section from Z_n to H.

In energy transfers, radiative heat exchanges and solar radiation are neglected. The contribution of internal heat gains (people, electrical appliances) is neglected. Referring to each i-th cell, the only heat flows are those related to the enthalpy carried by the interzonal mass flowrates (Eq. (5)) and the heat exchange with the outdoor environment through the building envelope by conduction and convection (Eq. (6)).

$$q_{ji} = \dot{m}_{ji}\, c_{p,air}\, \left(T_j - T_i\right) \tag{5}$$

$$q_{transm,i} = U\, A_{wall}\, \left(T_i - T_{air,ext}\right) \tag{6}$$

U is the thermal transmittance of the building structure and $T_{air,ext}$ is the external air temperature.

For each zone i, along with the ideal gas law, mass and energy balance equations are set under steady-state conditions (Eqs. (7)-(8)), obtaining a nonlinear system.

$$\sum \dot{m}_{ji} - \sum \dot{m}_{ij} + \dot{m}_{sup} - \dot{m}_{rem} = 0 \tag{7}$$

$$\sum q_{ji} - q_{transm,i} = 0 \tag{8}$$

After solving the system, the interzonal mass and volumetric flow rates can be explicitly computed reapplying the Power Law equations.

2.2 Risk assessment model

The airborne infection risk calculation is performed for each cell. The amount of aerosolised pathogens is expressed in terms of quanta. It is assumed that outdoor air does not contain infectious quanta. The infected source quanta exhalation rate is specific for the considered disease and indoor air becomes the carrier for the spread of these fictitious particles across the space. A quanta concentration balance (Eq. (9)) is set for each i-th cell:

$$V_i \frac{\mathrm{d}C_i}{\mathrm{d}t} = ER_i I_i - Q_{oi} C_i - \sum Q_{ij} C_i + \sum Q_{ji} C_j \tag{9}$$

where C is the zonal quanta concentration, ER is quanta emission rate for the disease, I is the number of infected people in the zone, Q_o is the exhaust air flow rate. The terms Q_{ij} and Q_{ji} represent the volumetric interzonal flow rates calculated from the zonal model.

Quanta concentrations represent the infectious material available at the breathing zone of a susceptible subject. Following the formulation given by Wells [8], the zonal infection risk $P_{I,i}$ for the susceptible individual is calculated through an exponential probability equation:

$$P_{I,i} = 1 - \mathrm{e}^{-p \int C_i(t)\mathrm{d}t} \tag{10}$$

where p is the breathing flow rate and t_{exp} is the exposure time interval. The exponent in Eq. (10) represents the intake dose of the susceptible subject.

2.3 Energy consumption calculation

A separate model was used for energy calculations. In addition, it was decided to distinguish between thermal and electrical consumptions; for this reason, two different calculation methods were defined and will be explained in this section.

The first step for the energy calculations was the definition of the HVAC system layout. In all the simulated environments, an ideal hydronic heating system was considered, which maintains the indoor conditions at 20°C temperature and 50% relative humidity; in addition to the heating system, a primary air mechanical ventilation system provides fresh external air to ensure high indoor air quality levels and infection risk mitigation. According to recent recommendations on airborne infection by the leading associations dealing with HVAC [14], the considered system does not include the possibility of air recirculation. Instead, the air is taken from outdoor and, after filtering, enters the air-handling unit (AHU), where it undergoes appropriate transformations. In heating conditions, the external air meets a crossflow heat exchanger where sensible heat recovery occurs, pre-heating coils, adiabatic saturator and post-heating coils, which bring it to the inlet conditions. Air is supplied to the room through two wall air diffusers, and two wall exhaust grilles near the floor were considered; inlets and outlets are placed at opposite sides of the room.

Inlet conditions were set and considered constant during the heating season: the air was supposed to enter the room at 20°C and 50% relative humidity. As for external conditions, monthly-average values were assumed for the external air temperature and the partial vapour pressure from the Italian Standard for Padova [15]. The values used for calculations are reported in Tab. 1.

Tab. 1 – Monthly average external air temperatures and vapour partial pressure.

Month	$p_{v\,ext}$	$T_{ext\,air}$
January	591 Pa	1.9 °C
February	652 Pa	4.0 °C
March	609 Pa	8.4 °C
November	934 Pa	8.2 °C
December	677 Pa	3.6 °C

According to the AHU layout, air undergoes four transformations. Among them, three sensible heating processes occur. The first one is due to the heat recovery (recuperator efficiencies η range between 80% and 98% as function of the volumetric flow rate), the other two when the air meets the pre- and post-heating heat exchangers. Finally, the humidification process is carried out between the pre- and post-heating processes by a saturator, working at constant efficiency (ε) equal to 90%.

Thermal energy demand consists of the energy supplied to the fresh air by the two heating coils. The energy used by the saturator has been neglected. The total energy supplied to the air is shown in Eq. (11).

$$E_{heating} = \dot{m}_{air}\,[(h_R - h_B) + (h_{IN} - h_C)]\,t \quad (11)$$

where $\dot{m}_{air}$ is the supply mass flow rate, h is the air specific enthalpy after the heat recovery (subscript R), after pre-heating coils (subscript B), after adiabatic saturator (subscript C) and after post-heating coils (subscript IN) and t is the operating time.

The electrical consumption was calculated assuming two variable speed fans for supply and return paths. The pressure drop due to continuous and localised effect was calculated; their aggregation provided a final value of the pressure drop, which was used for the choice of the electrical fans used for energy calculation.

Concerning distributed pressure drops, the airflow rate in a circular pipe was considered. According to the volume of the case study and, consequently, to the volumetric flow rates required, different duct diameters were chosen from commercial catalogues in order to maintain air velocities below a typical threshold of 10 m/s. Considering all cases, a range between 0.5 and 9 m/s was kept with this selection. In both supply and return paths, the pipe length was considered equal to 10 m. The choice of the same pipe length for all the considered AHUs is aimed at the comparison between different consumptions; therefore, it does not necessarily represent a realistic value for the considered system.

The components of the AHU were considered to generate a localised pressure drop that has been calculated assuming a quadratic relationship with mass flow rate (Eq. (12)):

$$\Delta P = \lambda\, Q^2 \quad (12)$$

The λ-values were extracted from datasheets of commercially available components. The pressure drop for each AHU can be seen in Tab. 2. For energy calculations, two different fans were considered for the supply and return paths; for the sake of simplicity, values reported in the table are the sum between them, considering both distributed and concentrated pressure drop.

Tab. 2 – Pressure drops in the supply and return paths of the AHU.

Air Changes per hour [h^{-1}]	Office Room	High school classroom	University classroom
0.5	23 Pa	28 Pa	43 Pa
1	53 Pa	72 Pa	97 Pa
1.5	94 Pa	132 Pa	150 Pa
2	145 Pa	223 Pa	229 Pa
2.5	198 Pa	321 Pa	324 Pa
3	258 Pa	445 Pa	434 Pa
3.5	332 Pa	598 Pa	560 Pa
4	422 Pa	760 Pa	710 Pa

3. Case Studies

3.1 Description and boundary conditions

The model described in the previous section was applied to three different case studies, representing an office room, a school classroom and a university classroom in heating conditions.

In all the analysed cases, the rooms are considered square or rectangular plants, with one vertical wall facing outside, whose thermal transmittance is equal to 0.3 $Wm^{-2}K^{-1}$. The presence of windows is not considered in the model, and infiltrations are also neglected. Dimensions and geometrical characteristics of the case studies are summarised in Tab. 3. As it can be seen, the three analysed volumes are very different from each other to evaluate the incidence of the proposed solutions in different volume rooms. Different occupancy profiles were applied according to the intended use of the building, as shown in Tab. 3. As explained in Section 2.1, the presence of occupants is only aimed at the infection risk assessment.

For all the case studies, the risk zonal model has been applied subdividing the geometrical domain into four identical well-mixed cells with a cross-section on the plan view, as shown in Fig. 2.

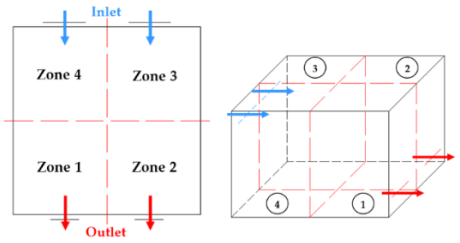

Fig. 2 – Discretisation grid applied to all case studies.

The same inputs of the risk model are set for all the analysed cases. The presence of one COVID-19 asymptomatic infected subject in Zone 1 is considered. The occupants' exhalation characteristics are assumed considering a sedentary activity, following [16]; thus, their breathing flow rate was set at 0.54 $m^3\ h^{-1}$ and, for the infected subject, a pathogen emission of 20 quanta/h was considered. The exposure time for the analysed cases was established according to the room final use, dealing with 8, 5 and 2 hours exposure time for the office workers, the high school and university students, respectively.

3.2 Sensitivity analysis

A sensitivity analysis was performed to highlight the influence of different aspects on ventilation costs and risk assessment. Despite the room volume, already mentioned in the previous section, the impact of varying renewal air flowrate and mask use was studied.

For each analysed case, the ventilation flowrate was ranged between 0.5 h^{-1} and 4 h^{-1}, with 0.5 h^{-1} steps. As already pointed out in Section 2.3, all the indicated air changes per hour assume 100% outdoor air.

Three different scenarios were outlined for the mask impact: in the first one, it was assumed that occupants were not wearing a mask; in the other two cases, the wearing of surgical and FFP2 masks was considered. For FFP2 masks, a penetration of the filter material of 6% and a leakage factor of 11% were obtained from European Standard [17]. According to Standard EN 14683:2019, surgical masks have a bacterial filtration efficiency of 95% in exhalation [18]. For the inhalation efficiency, the Standard does not indicate a value; for this reason, a precautionary value of 20% was chosen. Finally, a leakage factor of 27% for surgical masks was adopted according to [19].

4. Results and Discussion

4.1 Flow rate effect on risk and energy need

The effect of different ventilation flow rates in both the energy consumption and infection risk is analysed in this section. The probability of infection reported is the average between the values of the airborne infection risk in the four zones. This approach is justified by the similarity between risk values of the four cells; this aspect will be further discussed in Section 4.2. A permanent stay of both the susceptible subjects and the infective source inside the considered place for the duration of exposure time is assumed. As for energy consumption, the values reported for both thermal and electrical parts are calculated considering the seasonal operation of the AHU in steady conditions and at fixed mass flow rate. Daily consumption was calculated based on the exposure time for each case study; hence, monthly and seasonal consumptions were derived from the aggregation of daily values.

The simulation results for the office room are shown in Fig. 3. As the ventilation rate increases, there is a significant drop in the infection risk from 95% for 0.5 h^{-1} to 35% with 4 h^{-1}. Two relevant aspects can be highlighted in this case: the energy consumption grows significantly, up to almost ten times, but they represent only part of the total consumption, as they neglect the expenditure for heating purposes; moreover, it can be observed that, despite the high ventilation rate (considering 4 workers inside the office, the maximum flow rate analysed corresponds to about 13 L/s per person), with 8 hours continuous occupancy, the AHU alone cannot ensure enough fresh air to guarantee a healthy and safe workplace. For this reason, in cases of little offices similar to the analysed one, not only good ventilation must be provided, but also the correct use of personal protective equipment (PPE) must be observed. The specific thermal energy demand goes from about 10 kWh per person with 0.5 h^{-1} (1.7 L/s per person) to 102 kWh per person with 4 h^{-1} (13.4 L/s per person), whereas the specific electrical energy consumption goes from 0.5 to 81 kWh per person.

In the high school classroom (Fig. 4), the trend is the same respect to the office case: the increase of ventilation rate from 0.5 to 4 h^{-1} (e.g. from 0.8 to 6.1 L/s per person) leads to a decrease of infection risk (from 37% to 7%) with the annual consumption rising from 89 kWh to 948 kWh for thermal and from 2 kWh to 608 kWh for electrical share.

Tab. 3 – Case studies characteristics.

Room end-use	Dimensions					Occupancy
	L [m]	W [m]	H [m]	A_{floor} [m^2]	V [m^3]	
Office	4	4	3	16	48	4
High school classroom	8	6	3	48	144	26
University classroom	20	10	5	200	1000	151

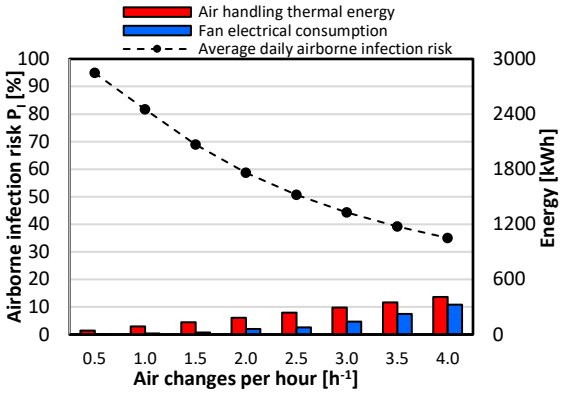

Fig. 3 – Daily infection risk (%), seasonal air handling thermal energy and fan electrical consumption (kWh) in the office case study.

The corresponding range of the specific energy demand lies between about 3 and 34 kWh per person for the required heating at the AHU finned coils, and between 0.1 and 23 kWh per person for fan absorption. Differently from the previous case, lower infection risk is detected; therefore, in this case, the volume effect is positive in terms of risk mitigation. On the other hand, it involves more considerable energy costs due to the higher volumetric flow rates needed to satisfy the required hourly changes.

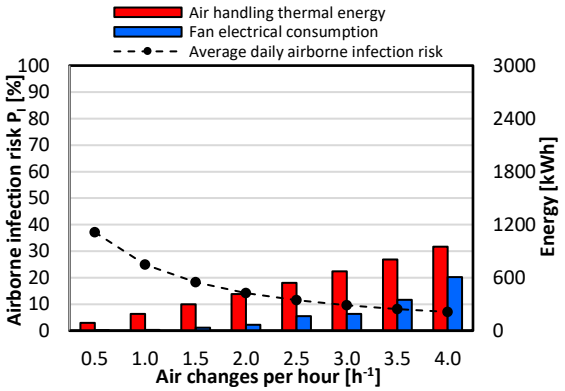

Fig. 4 – Daily infection risk (%), seasonal air handling thermal energy and fan electrical consumption (kWh) in the high school classroom.

The university classroom (Fig. 5) is the higher volume indoor environment simulated. As already shown for the other cases, the risk of infection is much lower than in the other rooms and energy consumption are greater. However, it should be noticed that the exposure time was considered equal to 2 h: this contributes to low values of infection probability, but extending the operation to other hours of the day, as is probable when considering a classroom used all day, would result in a further increase in consumption. As regards energy costs, the increase of ventilation flow rate from 0.5 to 4 h^{-1} (from 0.9 to 7.4 L/s per person) takes to an estimation of the specific thermal energy demand ranging from about 2 to 16 kWh per person and an electrical absorption between 0.1 and 10 kWh per person.

Similarly to the other cases, it can be concluded that the increase of the ventilation flow rate takes to higher energy costs but involves a decrease in the infection risk which passes from 1.3% to 0.3%.

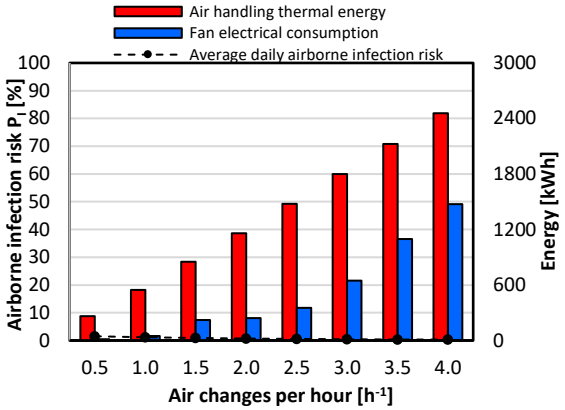

Fig. 5 – Daily infection risk (%), seasonal air handling thermal energy and fan electrical consumption (kWh) in the university classroom.

In this analysis, the occupants were considered not wearing masks; this aspect will be treated in the next section. Another aspect was not considered in this work: in higher volume places, the infection risk seems not crucial; however, high occupancy is likely to make it less realistic to employ only one infected person in the environment.

4.2 Relative position and mask effect

This section deals with assessing the probability of infection from COVID-19 obtained applying the zonal model. The risk extent is affected by different parameters, and their relevance is investigated.

As shown by the results reported in Section 4.1, an increase in the supply of outdoor air and higher room volumes lead to significant benefits in terms of infection risk since they promote the dilution of the airborne infectious material within the indoor space lowering its concentration to less harmful levels.

On the other hand, Fig. 6 shows the effect of the relative position between the infected source and the susceptible subjects, highlighting the spatial distribution of infection risk across the adopted grid through the zonal approach. The results are only reported for the single office room considering the extreme ventilation regimes (0.5 and 4 h^{-1}). Intermediate situations are trivially detected for the other flow rates.

The adopted calculation mesh defines a perfectly mixed environment. Therefore, the final infection risk is almost uniform within the space, and people's relative positions have limited effect. However, it can be noticed that spatial distribution of risk is slightly more heterogeneous with higher ventilation flow rates. Similar outcomes have been observed for the other case studies.

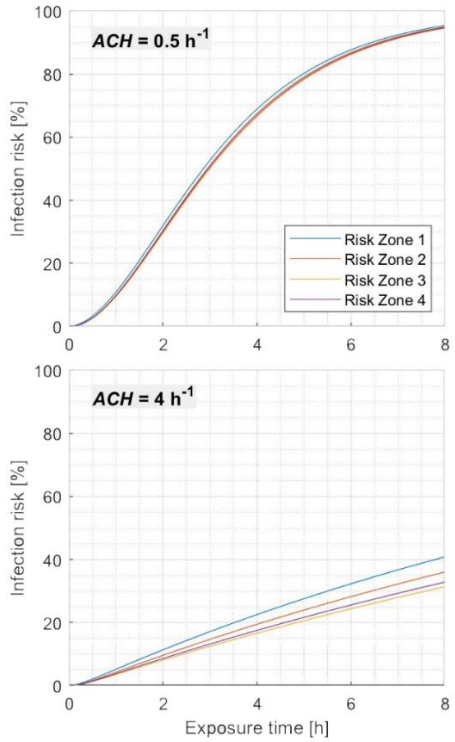

Fig.6 - Spatial distribution of risk in the office room.

Finally, Fig. 7 displays the risk curves obtained with both the infected and the susceptible subjects wearing the same type of mask. The shown situation is the worst one, i.e., a single office room (smallest volume) with an air change rate of 0.5 h^{-1} (lowest supply flow rate) and susceptible subject in Zone 1 (where the infected source is located).

The positive effect of using personal protective equipment is evident, even in this case. The infection spread is drastically reduced from a probability of 95 % without masks to 55 % with surgical masks and 8 % with FFP2. However, Fig. 7 points out that masks use must be coupled with adequate ventilation to maintain the risk below an acceptable threshold for smaller rooms.

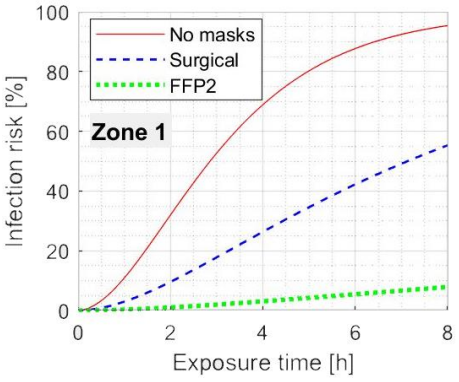

Fig. 7 – Influence of mask use on infection risk (office room, 0.5 h^{-1}, Zone 1).

For all the other situations, the benefits of masks are even more remarkable, also when the same exposure time is considered for comparison. Making the use of FFP2 devices mandatory could bring some advantages in energy consumption because lower flow rates would be sufficient to mitigate the airborne transmission of COVID-19. However, this aspect is out of the scope of this work.

5. Conclusions

In this work, the relationship between ventilation flow rate, energy consumptions and the risk of COVID-19 airborne infection was studied in three different indoor environments, a 48 m^3 office room, a 144 m^3 high school classroom and a 1000 m^3 university classroom. The effects of occupants' relative position inside the room, mask use and room volume on risk were also evaluated. For this purpose, a risk zonal model and an energy consumption model were applied to the considered case studies.

The following results emerged from this study:

- The increase of ventilation flow rate is an effective way to reduce the infection risk in indoor environments; however, it involves significant increases in energy consumption.
- With 8 hours exposure time, in the office case study the ventilation alone is not able to guarantee a safe and healthy workplace; in this context, the mask use can reduce the infection risk from 95% to 55% considering surgical masks and less than 10% with FFP2 masks (with 0.5 h^{-1} ventilation flowrate).
- The analysis of risk variation with relative position highlights a substantially uniform environment; to further analyse this aspect, a more discretised grid should be used in the model.

The proposed model presents some limitations and needs further improvements. A spatial modelling of jets and thermal plumes from heat sources can be included and a denser discretisation grid would be more appropriate to determine their effect on the mixing level of the indoor air. Additionally, the respiratory jets were not modelled, since people were considered as point sources of infectious aerosol; including information about temperature and momentum of exhalation jet would be suitable to get more accurate results from this type of analysis. Moreover, the likelihood of having more than one infected source in spaces with high occupancy should be considered.

6. Nomenclature

SYMBOL

A	Boundary surface area	m^2
ACH	Air changes per hour	h^{-1}
C	Quanta concentration	quanta m^{-3}
c_p	Specific heat at constant pressure	J kg^{-1} K^{-1}
E	Energy	kWh
ER	Quanta emission rate	quanta h^{-1}
g	Gravitational acceleration	m s^{-2}
h	Air specific enthalpy	kJ kg_{da}^{-1}
I	Number of infected sources	-

λ	Overall friction factor	Pa m^{-3} h
k	Flow coefficient	m s^{-1} Pa^{-n}
L	Depth of vertical boundary	m
$\dot{m}$	Mass flow rate	kg s^{-1}
P_I	Airborne infection probability	%
p	Breathing flow rate	m^3 h^{-1}
p_v	Partial vapour pressure	Pa
Q	Volumetric flow rate	m^3 h^{-1}
q_h	Heat flow	W
T	Temperature	K
t	Time	h
U	Thermal transmittance	W m^{-2} K^{-1}
V	Room volume	m^3
X	Mask filtration efficiency	%
Y	Leakage factor	%
Z_n	Height of the neutral plane	m
ΔP	Pressure difference	Pa
$\Delta\rho$	Air density difference	kg m^{-3}

Subscript

exh	exhalation
exp	exposure
ext	external
i	*i*-th zone
inh	inhalation
j	*j*-th zone
ref	reference level of zones (bottom level)
sup	supplied

7. References

[1] Eurostat, Energy data 2020 edition: Statistical book.

[2] Morawska L., Cao J. Airborne transmission of SARS-CoV-2: The world should face the reality. Environ. Int. 2020;139:105730.

[3] Morawska L., Tang J.W., Bahnfleth W., et al. How can airborne transmission of COVID-19 indoors be minimised? Environ. Int. 2020;142:105832.

[4] Buonanno G., Stabile L., Morawska L. Estimation of airborne viral emission: Quanta emission rate of SARS-CoV-2 for infection risk assessment. Environ. Int. 2020;141:105794.

[5] Miller S.L., Nazaroff W.W., Jimenez J.L., Boerstra A., et al. Transmission of SARS-CoV-2 by inhalation of respiratory aerosol in the Skagit Valley Chorale superspreading event. Indoor Air. 2021;31:314–323.

[6] Aliabadi A.A., Rogak S.N., Bartlett K.H., Green S.I. Preventing Airborne Disease Transmission: Review of Methods for Ventilation Design in Health Care Facilities. Adv. Prev. Med. 2011;2011:1–21.

[7] Ai Z.T., Melikov A.K. Airborne spread of expiratory droplet nuclei between the occupants of indoor environments: A review. Indoor Air. 2018;28:500–524.

[8] Sze To G.N., Chao C.Y.H. Review and comparison between the Wells-Riley and dose-response approaches to risk assessment of infectious respiratory diseases. Indoor Air. 2010;20:2–16.

[9] Schibuola L., Tambani C. High energy efficiency ventilation to limit COVID-19 contagion in school environments. Energy Build. 2021;240:110882.

[10] Wang J., Huang J., Feng Z., Cao S.J., Haghighat F. Occupant-density-detection based energy efficient ventilation system: Prevention of infection transmission. Energy Build. 2021;240: 110883.

[11] Noakes C.J., Sleigh P.A. Mathematical models for assessing the role of airflow on the risk of airborne infection in hospital wards. J. R. Soc. Interface. 2009;6:791-800.

[12] Lu Y., Dong J., Liu J. Zonal modelling for thermal and energy performance of large space buildings: A review. Renew. Sustain. Energy Rev. 2020;133:110241.

[13] Haghighat F., Li Y., Megri A.C. Development and validation of a zonal model - POMA. Build. Environ. 2001;36:1039–1047.

[14] Kurnitski J., Boerstra A., Franchimon F. COVID19 HVAC Guidance version 4.1. REHVA. 2021.

[15] Italian Organisation for Standardisation. Heating and cooling of buildings - Climate data: UNI 10349:2016.

[16] Buonanno G., Morawska L., Stabile L. Quantitative assessment of the risk of airborne transmission of SARS-CoV-2 infection: Prospective and retrospective applications. Environ. Int. 2020;145:106112.

[17] European Committee for Standardization - CEN. Respiratory protective devices - Filtering half masks to protect against particles - Requirements, testing, marking: EN 149:2001+A1:2009.

[18] European Committee for Standardization - CEN. Medical face masks. Requirements and test methods: EN 14683:2019.

[19] Mueller A.V., Eden M.J., Oakes J.M., Bellini C., Fernandez L.A. Quantitative Method for Comparative Assessment of Particle Removal Efficiency of Fabric Masks as Alternatives to Standard Surgical Masks for PPE. Matter. 2020;3:950–962.

Data Statement

Data sharing not applicable to this article as no datasets were generated or analysed during the current study.